J. Cryst. Growth 480 (2017) 78-84.

A comparative study of heterostructured CuO/$CuWO_4$ nanowires and thin films

Boris Polyakov[1,*], Alexei Kuzmin[1], Sergei Vlassov[1,2], Edgars Butanovs[1], Janis Zideluns[1], Jelena Butikova[1], Robert Kalendarev[1], Martins Zubkins[1]

[1] Institute of Solid State Physics, University of Latvia, Kengaraga street 8, LV-1063 Riga, Latvia

[2] Institute of Physics, University of Tartu, Ostwaldi 1, 50411 Tartu, Estonia

*Corresponding author: boris@cfi.lu.lv

Abstract. A comparative study of heterostructured CuO/$CuWO_4$ core/shell nanowires and double-layer thin films was performed through X-ray diffraction, confocal micro-Raman spectroscopy and electron (SEM and TEM) microscopies. The heterostructures were produced using a two-step process, starting from a deposition of amorphous WO_3 layer on top of CuO nanowires and thin films by reactive DC magnetron sputtering and followed by annealing at 650°C in air. The second step induced a solid-state reaction between CuO and WO_3 oxides through a thermal diffusion process, revealed by SEM-EDX analysis. Morphology evolution of core/shell nanowires and double-layer thin films upon heating was studied by electron (SEM and TEM) microscopies. A formation of $CuWO_4$ phase was confirmed by X-ray diffraction and confocal micro-Raman spectroscopy.

Keywords:
A1. Characterization
A1. Crystal morphology
A1. Nanostructures
B1. Oxides
B1. Tungstates

1. Introduction

Metal oxide nanowires (NWs) and their heterostructures are promising materials for the next generation of solar power harvesting devices [1,2], photocatalyst materials for water splitting [3,4] and gas sensing devices [5]. The use of axially heterostructured or core/shell NWs has several important advantages in comparison to thin film technologies: combination of materials with large lattice mismatch and even epitaxial growth of shell material on the core, improved mechanical properties due to a reduction in the number of defects per unit length, superior electroconductive properties of NWs due to their crystallinity and small defect concentration, large surface area and/or large heterojunction area, novel or significantly improved thermal, optical, electronic or field emission properties [6-10].

CuO nanowires can be produced in large quantities by simple and cost effective route of thermal oxidation of metallic copper or copper foil in air atmosphere [11]. A number of heterostructured core/shell NWs with CuO core were prepared and studied during last years.

The p-n CuO/ZnO heterojunction NWs were produced by thermal oxidation of copper and subsequent zinc oxide layer formation by atomic layer deposition [12] or thermal decomposition of zinc acetate [8, 13]. ZnO has a relatively large direct band gap of ~3.3 eV, similar to TiO_2 commonly used for photoelectrodes, but significantly enhanced electron mobility [14, 15]. Its combination with CuO, that has a narrow indirect band gap (1.2-1.4 eV), allows enhancing of light absorption in the solar spectrum region and solar conversion efficiency [8,13]. The sensing properties of CuO/ZnO NWs show higher sensitivity for reducing gases than those of pure CuO NWs [12]. Another successful application of CuO/ZnO NWs for solar energy harvesting and for hydrogen generation from photoelectrochemical water decomposition was demonstrated in [8, 13].

CuO/Co_3O_4 coaxial heterostructures, prepared by hydrothermal method, were studied in [16]. It was found that their morphology plays an important role in photocatalytic properties. In particular, coaxial heterostructures show higher photocatalytic efficiency under solar light irradiation compared with pure CuO nanorods and Co_3O_4 nanoflowers [16].

At the same time, the morphology of the CuO-core NWs can be often undesirably affected and totally disrupted by shell coating. For example, the coverage of straight CuO NWs with smooth surface by TiO_2-shell using metalorganic chemical vapour deposition technique led to NWs winding and roughening even at moderate substrate temperature 350°C [17]. Often NWs undergo severe shape and morphology degradation, or lose their integrity during chemical reactions in solid state [18,19]. This phenomenon of core degradation in CuO NWs is linked with diffusion of copper or oxygen atoms during chemical reaction and process of shell formation, and needs further investigation.

Recently $CuO/CuWO_4$ core/shell NW arrays were proposed as well-consisted system with enhanced activity and durability for photoelectrochemical water splitting (PEC) [20]. Pure $CuWO_4$ is a promising photoanode material, having electronic structure close to ideal for PEC water splitting [20-24]. It has n-type conductivity [25] with the indirect band gap in the range of 1.9-2.3 eV [26, 27, 28, 29, 30, 31]. $CuWO_4$ layer was produced on top of CuO NW array in solid-state chemical reaction employing hot wire chemical vapour deposition technique using tungsten and copper wires as a source of both tungsten oxide and copper/copper oxide vapours. The underlying CuO nanowires become essentially pure Cu_2O after deposition. It was shown [20] that the presence of $CuWO_4$ shell improves the photocurrents of Cu_2O NWs by improving their phase purity and charge separation due to the formation of a high-quality p-n heterojunction. However, no data of internal morphology of heterostructured NWs was provided in [20].

p-CuO/n-$CuWO_4$ heterojunction thin films were prepared recently using a multi-step process [32]. First, copper film was electrodeposited and annealed in air to obtain CuO film. Next, $CuWO_4$ layer was produced by spin-coating of tungstic acid and subsequent annealing at 500°C for 2 h in air. However, such synthesis approach resulted in largely irregular morphology of the heterojunction layer [32].

In this study, we investigated the formation mechanism and morphology evolution of two structures – 1D $CuO/CuWO_4$ core/shell NWs and 2D double-layer $CuO/CuWO_4$ thin films

prepared by reactive DC magnetron sputtering and post annealing in air. A comparison of two structures was performed in order to understand the mechanism of $CuWO_4$ phase formation upon annealing. Note that due to technical difficulties it is challenging to compare the same nanowire before and after annealing, while compositional and morphological analysis of thin film cross section before and after annealing is straightforward. X-ray diffraction (XRD), electron microscopy methods, confocal micro-Raman spectroscopy and spatial energy dispersive X-ray (EDX) analysis allowed us to figure out details of $CuWO_4$ formation process. To the best of our knowledge, this is the first comparison of a transformation from CuO/WO_3 to $CuO/CuWO_4$ in core/shell NWs and thin films upon heating.

2. Experimental details

Core/shell nanowire synthesis (sample type 1). An array of CuO NWs was grown by heating copper foil at 450°C in a high temperature oven (Carbolite HTF 17/5) over a period of two hours [33]. Synthesized NWs were 10-20 μm long, with diameters in the range of 30 to 150 nm. Then the array of CuO NWs was coated by a layer (100 nm on flat substrate) of amorphous WO_3 using reactive DC magnetron sputtering at room temperature of metallic tungsten target in mixed Ar(80%)-O_2(20%) atmosphere [34] (sample type 1, Fig. 1). Core/shell CuO/WO_3 NWs samples were annealed for two hours at 650°C to induce a formation of $CuWO_4$ shell via the solid-state reaction between CuO NW and amorphous WO_3 layer.

Double-layer thin film synthesis (sample type 2). Double-layer CuO/WO_3 thin film was deposited on Si(100) wafer substrate by reactive DC magnetron sputtering method consecutively from Cu (99.99%) and metallic W (99.95%) targets in mixed argon-oxygen atmosphere. The deposition was performed at a power of 200 W and a pressure of 20 mTorr. The target to substrate distance was about 9 cm, and the substrate was not heated intentionally. The Ar and O_2 gas flow rates were kept constant at 20 sccm and 10 sccm, respectively. Thus obtained WO_3/CuO/Si(100) sample (sample type 2, Fig. 1) was cut into two parts, and one part was heated in a horizontal tube

furnace at about 650°C for two hours in air to induce a reaction between the two oxide layers leading to a formation of $CuWO_4$.

Characterization. The crystallographic structure of heterostructured CuO/WO_3 NWs and double-layer thin films was characterized by X-ray diffraction (XRD). XRD measurements were carried out at room temperature using X-ray diffractometer X'Pert Pro Powder (PANalytical) with a Cu-Kα source by scanning θ-θ in the range of 10-60°.

The morphology and elemental composition of amorphous WO_3-coated CuO NWs and annealed core/shell CuO/WO_3 NWs were studied using a high-resolution scanning electron microscope (SEM Lyra, Tescan) equipped with Oxford instruments energy dispersive X-ray (EDX) detector X-Max 50 mm^2 operated at 15 keV. The inner structure of core/shell NWs was investigated by a high-resolution transmission electron microscope (HRTEM Tecnai GF20, FEI) operated at an accelerating voltage of 180 kV.

Micro-Raman spectroscopy measurements were performed using a confocal microscope with spectrometer Nanofinder-S (SOLAR TII) [35]. Polycrystalline CuO and $CuWO_4$ powders were also measured for comparison. A diode pumped solid-state (DPSS) Nd:YAG laser (532 nm, max CW power P_{ex}=150 mW) was used as the excitation source. A continuous neutral filter with the optical density (OD) in the range of OD=0-3 was used to attenuate laser beam: OD=0 corresponds to about 12 mW at the sample. A Peltier-cooled back-thinned CCD camera (ProScan HS-101H) was used to register Raman scattering spectra. Hamamatsu R928 photomultiplier tube was employed in confocal-spectral imaging experiments. All measurements were performed in back-scattering geometry at room temperature (20°C) through a Nikon CF Plan Apo 100× (NA=0.95) optical objective.

3. Results and discussion

3.1.Structural analysis

XRD patterns were recorded for oxidized copper foil covered with CuO NWs (Fig. 2a). During oxidation process copper foil is covered by a layer of Cu_2O followed by the next layer of CuO film with protruding CuO NWs. Vertical orientation of CuO NWs is favourable for deposition of other materials (WO_3 in our case) by sputtering techniques. Bragg peaks positions for as grown CuO NWs sample are typical for such samples [36]. Metallic copper, CuO and Cu_2O can be identified in Fig. 2a. XRD pattern of WO_3 coated CuO NWs is identical to pure CuO NWs (not shown on the graph) due to amorphous structure of WO_3 layer. After annealing at 650°C in air for two hours the signal from metallic copper disappears due to all copper is oxidized but a new signal from $CuWO_4$ phase appears [37, 38].

XRD patterns of untreated and heated WO_3/CuO/Si(100) thin films are shown in Fig. 2b. A sharp peak with a shoulder at about $2\theta=33°$ (labelled by asterisk in Fig. 2b) is a forbidden Si(200) reflection from the Si(100) wafer due to the multiple diffraction [39]. The pattern of a non-treated sample contains only CuO(11-1) broad peak indicating its textured nanocrystalline phase, whereas no evidence of WO_3 phase is present suggesting that it is in amorphous state, as expected. Upon heating at 650°C in air for two hours the crystallinity of CuO layer is improved, and the peak at 35.6° becomes less broadened. At the same time, a reaction between tungsten oxide and copper oxide layers occurs leading to a formation of $CuWO_4$ phase [37, 38].

3.2.Morphological analysis

A series of SEM images of pure CuO and WO_3-coated CuO NWs as well as core/shell CuO/WO_3 NWs annealed at 650°C in air are shown in Fig. 3. Pure CuO NWs have smooth faceted surface (Fig. 3a,b,c). After deposition of amorphous WO_3 layer a homogeneous shell is formed around CuO core with fine roughness (Fig. 3d). Further annealing of core/shell CuO/WO_3 NWs at 650°C leads to a crystallization of the outer shell and to a reaction between the core and the shell resulting in a formation of $CuWO_4$ phase (Fig. 3e-h).

An important question is how $CuWO_4$ is forming – either through Cu atoms diffusion into WO_3 layer or mutual interdiffusion of Cu and W atoms. Note that it is almost impossible to measure a change of CuO NW core diameter before and after annealing for the same CuO/WO_3 nanowire. However, in the case of double-layer CuO/WO_3 thin film it is possible to compare film thickness and morphology before and after annealing (Fig. 4). As-deposited CuO/WO_3 thin film before annealing has smooth surface (Fig. 4a), and in cross section, CuO and WO_3 layers are indistinguishable and appear as columnar and dense film (Fig. 4b). Annealed film has small voids and pores visible on the image from the top (Fig. 4e), and the two layers have clearly different morphology in cross section (Fig. 4f). Analysing EDX element maps of Cu and W atom distribution before and after annealing, one can see that tungsten atoms did not diffused into CuO layer, while copper atoms moved into the tungsten oxide layer, thus giving origin to $CuWO_4$ phase (Fig. 4c,d,g,h).

More detailed information on the internal microstructure of the same set of NW samples was obtained by TEM microscopy (Fig. 5). Pure CuO NWs have a perfect crystalline structure (Fig. 5a,b) with the measured interplanar distance of ~2.5 Å, corresponding to the (11-1) plane of CuO. Our DC magnetron sputtering of tungsten in oxidizing atmosphere on a substrate maintained at room temperature produces an amorphous WO_3 film [34]. Therefore, WO_3 layer in as-prepared core/shell CuO/WO_3 NWs is amorphous as expected (Fig. 5c,d). The thickness of amorphous WO_3 layer averaged over several NWs was approximately 50 nm.

Crystallization of outer layer in core/shell NWs was observed upon annealing at 650ºC (Fig. 5e,f). According to measured interplanar distance equal to 3.6 Å, the outer layer of NWs was identified as $CuWO_4$ phase with the (011) lattice planes [40,41]. This means that a solid-state reaction between amorphous WO_3 layer and CuO NW core occurred by thermal diffusion process. For comparison, monoclinic WO_3 [42] and $W_{18}O_{49}$ [43,44] nanowires have larger interplanar distances of about 3.8 Å for (001) and (010) planes, respectively. Upon annealing $CuWO_4$ crystals located around NWs core become self-assembled in a quasiperiodic manner (Fig. 5g,h). Note that

after annealing and formation of $CuWO_4$ crystals the CuO core remains single crystal phase and straight in shape (no voids are visible). Probably mostly copper atoms from the nanowire surface (as most mobile ones) move into WO_3 layer to form $CuWO_4$.

3.3.Raman spectroscopy

CuO [45], WO_3 [34] and $CuWO_4$ [46] crystalline phases can be easily distinguished according to their Raman response. Therefore, the use of confocal micro-Raman spectroscopy allowed us to access the phase composition of individual NWs and to follow their transformation upon annealing. Representative Raman spectra for individual as-prepared and annealed core/shell CuO/WO_3 NWs on silicon substrate, measured with full laser power (OD=0), are reported in Figs. 6b and 6d, respectively. Note that the first-order (~524 cm^{-1}) and second-order (~960 cm^{-1}) Raman bands from silicon substrate are also well observed, and their positions agree well with those from [47].

Raman scattering spectrum of pure CuO NW sample consists of phonon bands at 293 cm^{-1} (A_g mode), 339 cm^{-1} and 623 cm^{-1} (B_g modes) in agreement with [48,49] and also with bulk CuO [45]. The position of the main band at 293 cm^{-1} is strongly temperature-dependent [50]; therefore, its red-shift by ~22 cm^{-1} and broadening in polycrystalline CuO powder and core/shell CuO/WO_3 NWs is caused by local laser heating (Fig. 6d).

Raman scattering spectra of core/shell CuO/WO_3 NWs are dominated by a contribution from $CuWO_4$ phase (Fig. 6b,d). Crystalline $CuWO_4$ has triclinic structure (space group *P-1, Z=2*) [51] composed of CuO_6 and WO_6 octahedra, distorted by the first-order and second-order Jahn-Teller effects, respectively [29]. According to group theoretical analysis, 36 phonon modes are expected at the centre of Brillouin-zone in $CuWO_4$, and 18 of them are even Raman active A_g modes. The positions of Raman bands at 121, 218, 277, 309, 472, 730, 770 and 900 cm^{-1} (Fig. 5b,d) agree well with those in bulk $CuWO_4$ [29,46]. The appearance of $CuWO_4$ phase in Raman spectrum of as-prepared sample is due to solid-state reaction between nanowire CuO core and WO_3 shell induced locally by laser heating. This fact agrees well with literature data, where formation of crystalline

$CuWO_4$ from mixture of copper and tungsten salts starts approximately at 200ºC [31]. Note that the most pronounced Raman band at 900 cm^{-1}, related to symmetric stretching W–O vibration [29, 46], can be used as a fingerprint of $CuWO_4$ phase existence. Laser-induced formation of $CuWO_4$ opens the possibilities to modify locally core-shell nanowires by focused laser beam for a fabrication of nano-device prototypes.

As it was shown above by TEM and SEM, CuO core preserves its straight shape and single-crystalline structure after the formation of $CuWO_4$ shell. The work by Jun et al. [17] on the investigation of the synthesis of CuO/TiO_2 core-shell NWs demonstrated that CuO core loses its straight shape, and the resulting core-shell NWs are heavily deformed. A thorough study by Wu et al. [19] on the process of conversion of CuO NWs into Cu_2O NWs indicated that the core of a NW remains straight for a long time while Cu_2O nanocrystals grow on the NW walls. This fact gives evidence that the removal of a large number of atoms from NW core is not critical for preservation of straight shape of the core. In our system, CuO core was coated by continuous layer of amorphous WO_3, which converted into discontinuous $CuWO_4$ shell during annealing through diffusion route. It is possible that the discontinuous shell of $CuWO_4$ cannot generate stress strong enough to break CuO core in contrast to the continuous crystalline TiO_2 shell.

Raman scattering spectra of two WO_3/CuO/Si(100) samples are shown in Fig. 7. One should note that a care should be taken when measuring thin films due to a possibility of laser induced crystallization [33]. In fact, at low laser power (1.2 mW) the non-treated sample shows weak Raman activity, which is typical for amorphous WO_3 thin film [33]: only the band at 960 cm^{-1} due to a symmetric stretching mode of short terminal W=O bonds [52] is visible. Upon increasing laser power up to 12 mW, the top WO_3-layer crystallises, and its Raman spectrum becomes similar to those of WO_3 thin film annealed at 400°C [53] and of nanocrystaline WO_3 with the crystallites size of about 16-35 nm [54, 55]: several bands are visible at 128, 183, 262, 322, 690-700, 804 and 960 cm^{-1}. The origin of these bands is due to the stretching modes of the bridging oxygens ν(W-O-W) (the bands at 690-700 and 804 cm^{-1}), the bending (deformation) modes δ(O-W-O) at 262

and 322 cm^{-1} as well as the lattice modes at 128 and 183 cm^{-1} [2]. The Raman scattering spectrum of annealed sample has reach structure: most bands, including the main one at 906 cm^{-1}, are attributed to bulk $CuWO_4$ phase [29]. However, there is also the band due to silicon substrate at 525 cm^{-1} and some evidence of two bands due to CuO layer at 290 and 314 cm^{-1} [56]. The latter two bands overlap strongly with the bands of $CuWO_4$. Thus, the Raman data agree with the results of XRD analysis and confirm formation of $CuWO_4$ phase upon high temperature annealing.

4. Conclusions

In this paper we present the results of a comparative study of heterostructured CuO/$CuWO_4$ core/shell nanowires and double-layer thin films, which were synthesised by a simple approach based on a two-step process. Amorphous WO_3 thin layer was deposited first on top of CuO nanowires or thin film by reactive DC magnetron sputtering of tungsten, and high temperature annealing was used next to induce a solid-state reaction between CuO and WO_3 resulting in a formation of $CuWO_4$ phase. Note that similar approach can be employed for a production of other heterostructured metal-oxide/tungstate systems, such as NiO/$NiWO_4$ and ZnO/$ZnWO_4$ [57,58].

The morphology evolution of heterostructured core/shell nanowires and thin films upon heating was studied by scanning and transmission electron microscopies. A formation of crystalline $CuWO_4$ phase around nanowires or at the thin film surface was observed upon annealing of CuO/WO_3 system at 650ºC in air and is due to thermally stimulated diffusion of copper ions into outer WO_3 layer, as revealed by SEM-EDX analysis. Note that CuO nanowire core is able to provide sufficient amount of copper ions into the WO_3 shell to produce $CuWO_4$ and still preserves its integrity and straight shape. The emergence of $CuWO_4$ phase was confirmed by X-ray diffraction and confocal micro-Raman spectroscopy.

Acknowledgements

This work was supported by the Latvian National Research Program IMIS2. Authors are grateful to Reinis Ignatans for XRD measurements.

References

[1] T. J. Kempa, R. W. Day, S. Kim, H. Park, C. M. Lieber, Semiconductor nanowires: a platform for exploring limits and concepts for nano-enabled solar cells, Energy Environ. Sci. 6 (2013) 719-733.

[2] R. R. LaPierre, A. C. E. Chia, S. J. Gibson, C. M. Haapamaki, J. Boulanger, R. Yee, P. Kuyanov, J. Zhang, N. Tajik, N. Jewell, K. M. A. Rahman, III–V nanowire photovoltaics: Review of design for high efficiency, Phys. Status Solidi RRL 7 (2013) 815-830.

[3] Z. Li, W. Luo, M. Zhang, J. Feng, Z. Zou, Photoelectrochemical cells for solar hydrogen production: current state of promising photoelectrodes, methods to improve their properties, and outlook, Energy Environ. Sci. 6 (2013) 347-370.

[4] S. J. A. Moniz, S. A. Shevlin, D. J. Martin, Z. X. Guo, J. Tang, Visible-light driven heterojunction photocatalysts for water splitting – a critical review, Energy Environ. Sci. 8 (2015) 731-759.

[5] Z. Fan, J. C. Ho, T. Takahashi, R. Yerushalmi, K. Takei, A. C. Ford, Y. L. Chueh, A. Javey, Toward the development of printable nanowire electronics and sensors, Adv. Mater. 21 (2009) 3730-3743.

[6] Y. Xia, P. Yang, Y. Sun, Y. Wu, B. Mayers, B. Gates, Y. Yin, F. Kim, H. Yan, One-dimensional nanostructures: synthesis, characterization, and applications, Adv. Mater. 15 (2003) 353-389.

[7] P. J. Pauzauskie, P. Yang, Nanowire photonics, Mater. Today 9 (2006) 36-45.

[8] X. H. Zhao, P. Wang, B. J. Li, CuO/ZnO core/shell heterostructure nanowire arrays: synthesis, optical property, and energy application, Chem. Commun. (Camb.) 46 (2010), 6768-6770.

[9] P. Wang, X. Zhao, B. Li, ZnO-coated CuO nanowire arrays: fabrications, optoelectronic properties, and photovoltaic applications, Optics Express 19 (2011) 11271-11279.

[10] J. K. Wu, W. J. Chen, Y. H. Chang, Y. F. Chen, D. R. Hang, C. T. Liang, J. Y. Lu, Fabrication and photoresponse of ZnO nanowires/CuO coaxial heterojunction, Nanoscale Res. Lett. 8 (2013) 387.

[11] J. Liang, N. Kishi, T. Soga, T. Jimbo, The synthesis of highly aligned cupric oxide nanowires by heating copper foil, J. Nanomaterials 2011 (2011) 268508.

[12] J. H. Kim, A. Katoch, S. S. Kim, Optimum shell thickness and underlying sensing mechanism in p-n CuO-ZnO core-shell nanowires, Sens. Actuators B 222 (2016) 249-256.

[13] X. Zhao, P. Wang, Y. Gao, X. Xu, Z. Yan, N. Ren, CuO/ZnO core/shell nanowire arrays and their photovoltaics application, Mater. Lett. 132 (2014) 409-412.

[14] E. M. Kaidashev, M. Lorenz, H. von Wenckstern, A. Rahm, H. C. Semmelhack, K. H. Han, G. Benndorf, C. Bundesmann, H. Hochmuth, M. Grundmann, High electron mobility of epitaxial ZnO thin films on c-plane sapphire grown by multistep pulsed-laser deposition, Appl. Phys. Lett. 82 (2003) 3901-3903.

[15] E. Hendry, M. Koeberg, B. O'Regan, M. Bonn, Local field effects on electron transport in nanostructured TiO_2 revealed by terahertz spectroscopy, Nano Lett. 6 (2006) 755-759.

[16] R. X. Chen, S. L. Zhu, J. Mao, Z. D. Cui, X. J. Yang, Y. Q. Liang, Z. Y. Li, Synthesis of CuO/Co_3O_4 coaxial heterostructures for efficient and recycling photodegradation, Int. J. Photoenergy 2015 (2015) 183468.

[17] J. Jun, C. Jin, H. Kim, S. Park, C. Lee, Fabrication and characterization of CuO-core/TiO_2-shell one-dimensional nanostructures, Appl. Surf. Sci. 255 (2009) 8544-8550.

[18] L. Yuan, A. G. V. D. Geest, W. Zhu, Q. Yin, L. Li, A. N. Kolmogorov, G. Zhou, Reduction of CuO nanowires confined by a nano test tube, RSC Adv. 4 (2014) 30259-30266.

[19] F. Wu, Y. Myung, P. Banerjee. Rayleigh instability driven nodular Cu_2O nanowires via carbothermal reduction of CuO nanowires, Cryst. Growth Des. 15 (2015) 1588-1595.

[20] A. Martınez-Garcıa, V. Kalyan Vendra, S.i Sunkara, P. Haldankar, J. Jasinski, M. K. Sunkara, Tungsten oxide-coated copper oxide nanowire arrays for enhanced activity and durability with photoelectrochemical water splitting, J. Mater. Chem. A 1 (2013) 15235-15241.

[21] J. E. Yourey, B. M. Bartlett, Electrochemical deposition and photoelectrochemistry of $CuWO_4$, a promising photoanode for water oxidation, J. Mater. Chem. 21 (2011) 7651-7660.

[22] Y. Gao, O. Zandi, T. W. Hamann, Atomic layer stack deposition-annealing synthesis of $CuWO_4$, J. Mater. Chem. A 4 (2016) 2826-2830.

[23] J. C. Hill, K. S. Choi, Synthesis and characterization of high surface area $CuWO_4$ and Bi_2WO_6 electrodes for use as photoanodes for solar water oxidation, J. Mater. Chem. A 1 (2013) 5006-5014.

[24] S. K. Pilli, T. G. Deutsch, T. E. Furtak, L. D. Brown, J. A. Turner, A. M. Herring, $BiVO_4/CuWO_4$ heterojunction photoanodes for efficient solar driven water oxidation, Phys. Chem. Chem. Phys. 15 (2013) 3273-3278.

[25] T. Mathew, N. M. Batra, S. K. Arora, Electrical conduction in $CuWO_4$ crystals, J. Mater. Sci. 27 (1992) 4003-4008.

[26] P. K. Pandey, N. S. Bhave, R. B. Kharat, Spray deposition process of polycrystalline thin films of $CuWO_4$ and study on its photovoltaic electrochemical properties, Mater. Lett. 59 (2005) 3149-3155.

[27] R. Lacomba-Perales, J. Ruiz-Fuertes, D. Errandonea, D. Martınez-Garcıa, A. Segura, Optical absorption of divalent metal tungstates: Correlation between the band-gap energy and the cation ionic radius, EPL 83 (2008) 37002.

[28] Y. Chang, A. Braun, A. Deangelis, J. Kaneshiro, N. Gaillard, Effect of thermal treatment on the crystallographic, surface energetics, and photoelectrochemical properties of reactively cosputtered copper tungstate for water splitting, J. Phys. Chem. C 115 (2011) 25490-25495.

[29] A. Kuzmin, A. Kalinko, R.A. Evarestov, Ab initio LCAO study of the atomic, electronic and magnetic structures and the lattice dynamics of triclinic $CuWO_4$, Acta Mater. 61 (2013) 371-378.

[30] S. Dey, R. A. Ricciardo, H. L. Cuthbert, P. M. Woodward, Metal-to-metal charge transfer in AWO_4 (A= Mg, Mn, Co, Ni, Cu, or Zn) compounds with the wolframite structure, Inorg. Chem. 53 (2014) 4394-4399.

[31] E. L. S. Souza, C. J. Dalmaschio, M. G. R. Filho, G. E. Luz Jr., R. S. Santos, E. Longo, L. S. Cavalcante, Structural refinement and photocatalytic properties of $CuWO_4$ crystals, in Microscopy: advances in scientific research and education, Vol. 2, A. Méndez-Vilas (ed.) (Formatex Research Center, Badajoz, 2014), pp. 894-902.

[32] J. Y. Zheng, G. Song, C. W. Kim, Y. S. Kang, Facile preparation of p-CuO and p-CuO/n-$CuWO_4$ junction thin films and their photoelectrochemical properties, Electrochim. Acta 69 (2012) 340-344.

[33] X. Jiang, T. Herricks, Y. Xia, CuO nanowires can be synthesized by heating copper substrates in air, Nano Lett. 2 (2002) 1333-1338.

[34] A. Kuzmin, R. Kalendarev, A. Kursitis, J. Purans, Confocal spectromicroscopy of amorphous and nanocrystalline tungsten oxide films, J. Non-Cryst. Solids 353 (2007) 1840-1843.

[35] A. Kuzmin, R. Kalendarev, A. Kursitis, J. Purans, Confocal spectromicroscopy of micro and nano-structured materials, Latvian J. Phys. Technol. Sci. 2 (2006) 66.

[36] A. Othonos, M. Zervos, Ultrafast hole carrier relaxation dynamics in p-type CuO nanowires, Nanoscale Res. Lett. 6 (2011) 622.

[37] J. B. Forsyth, C. Wilkinson, A. I. Zvyagin, The antiferromagnetic structure of copper tungstate, $CuWO_4$, J. Phys.: Condens. Matter 3 (1991) 8433-8440.

[38] P. F. Schofield, S. A. T. Redfern, Ferroelastic phase transition in the sanmartinite ($ZnWO_4$)-cuproscheelite ($CuWO_4$) solid solution, J. Phys.: Condens. Matter 4 (1993) 375-388.

[39] P. Zaumseil, High-resolution characterization of the forbidden Si 200 and Si 222 reflections, J. Appl. Cryst. 48 (2015) 528-532.

[40] C. L. Li, Z. W. Fu, Nano-sized copper tungstate thin films as positive electrodes for rechargeable Li batteries, Electrochim. Acta 53 (2008) 4293-4301.

[41] A. Thomas, C. Janky, G. F. Samu, M. N. Huda, P. Sarker, J. P. Liu, V. van Nguyen, E. H. Wang, K. A. Schug, K. Rajeshwar, Time- and energy-efficient solution combustion synthesis of binary metal tungstate nanoparticles with enhanced photocatalytic activity, ChemSusChem 8 (2015) 1652-1663.

[42] Y. Baek, K. Yong, Controlled growth and characterization of tungsten oxide nanowires using thermal evaporation of WO_3 powder, J. Phys. Chem. C 111 (2007) 1213-1218.

[43] J. Zhou, L. Gong, S. Z. Deng, J. Chen, J. C. She, N. S. Xu, Growth and field-emission property of tungsten oxide nanotip arrays, Appl. Phys. Lett. 87 (2005) 223108.

[44] R. Seelaboyina, J. Huang, Multistage field enhancement of tungsten oxide nanowires and its field emission in various vacuum conditions, Nanotechnology 17 (2006) 4840-4844.

[45] H. Hagemann, H. Bill, W. Sadowski, E. Walker, M. François, Raman spectra of single crystal CuO, Solid State Commun. 73 (1990) 447-451.

[46] J. Ruiz-Fuertes, D. Errandonea, R. Lacomba-Perales, A. Segura, J. González, F. Rodríguez, F. J. Manjón, S. Ray, P. Rodríguez-Hernández, A. Muñoz, Zh. Zhu, C. Y. Tu, High-pressure structural phase transitions in $CuWO_4$, Phys. Rev. B 81 (2010) 224115.

[47] P. A. Templet, C. E. Hathaway, Multiphonon Raman spectrum of silicon, Phys. Rev. B 7 (1973) 3685-3697.

[48] J. F. Xu, W. Ji, Z. X. Shen, W. S. Li, S. H. Tang, X. R. Ye, D. Z. Jia, X. Q. Xin, Raman spectra of CuO nanocrystals, J. Raman Spectrosc. 30 (1999) 413-415.

[49] M. H. Chou, S. B. Liu, C. Y. Huang, S. Y. Wu, C. L. Cheng, Confocal Raman spectroscopic mapping studies on a single CuO nanowire, Appl. Surf. Sci. 254 (2008) 7539-7543.

[50] S. Ravi, A. B. Kaiser, C. W. Bumby, Effect of temperature and micro-morphology on the Ag Raman peak in nanocrystalline CuO thin films, J. Appl. Phys. 118 (2015) 085311.

[51] L. Kihlborg, E. Gebert, $CuWO_4$, a distorted wolframite-type structure, Acta Cryst. B 26 (1970) 1020-1025.

[52] M. F. Daniel, B. Desbat, J. C. Lassegues, B. Gerand, M. Figlarz, Infrared and Raman study of WO_3 tungsten trioxides and WO_3,xH_2O tungsten trioxide hydrates, J. Solid State Chem. 67 (1987) 235-247.

[53] E. Ozkana, S.-H. Lee, C. E. Tracy, J. R. Pitts, S. K. Deb, Comparison of electrochromic amorphous and crystalline tungsten oxide films, Sol. Energy Mater. Sol. Cells 79 (2003) 439-448.

[54] M. Boulova, G. Lucazeau, Crystallite nanosize effect on the structural transitions of WO_3 studied by Raman spectroscopy, J. Solid State Chem. 167 (2002) 425-434.

[55] M. Boulova, A. Gaskov, G. Lucazeau, Tungsten oxide reactivity versus CH_4, CO and NO_2 molecules studied by Raman spectroscopy, Sens. Actuators B 81 (2001) 99-106.

[56] H. F. Goldstein, D. Kim, P. Y. Yu, L. C. Bournet, Raman study of CuO single crystals, Phys. Rev. B 41 (1990) 7192-7194.

[57] Y. Wang, L. Cai, Y. Li, Y. Tang, C. Xie, Structural and photoelectrocatalytic characteristic of ZnO/$ZnWO_4$/WO_3 nanocomposites with double heterojunctions, Physica E 43 (2010) 503-509.

[58] B. R. Huang, T. C. Lin, K. T. Chu, Y. K. Yang, J. C. Lin, Field emission properties of zinc oxide/zinc tungstate (ZnO/$ZnWO_4$) composite nanorods, Surf. Coat. Technol. 231 (2013) 289-292.

Figures

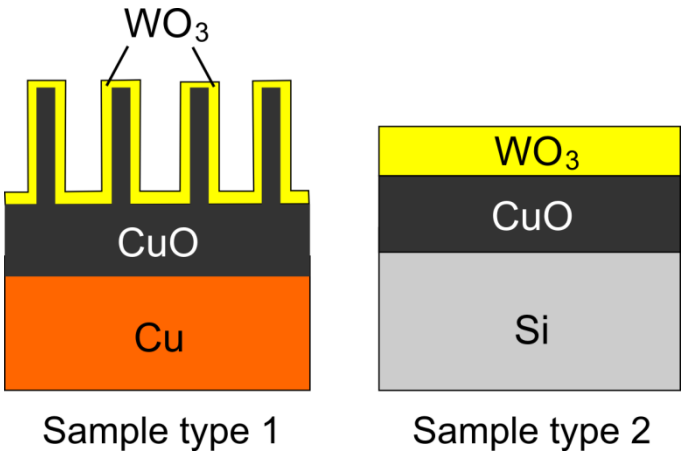

Fig. 1. Schematics of core-shell nanowire samples and double-layer thin film samples.

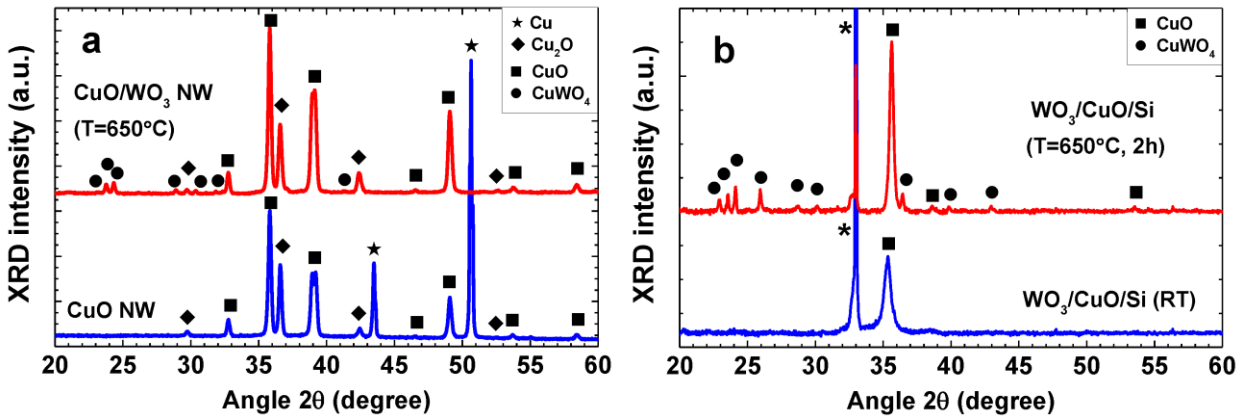

Fig. 2. XRD patterns of CuO NWs grown on Cu foil and CuO/WO_3 NWs annealed at 650°C (a), and CuO/WO_3 thin film before and after annealing at 650°C (b).

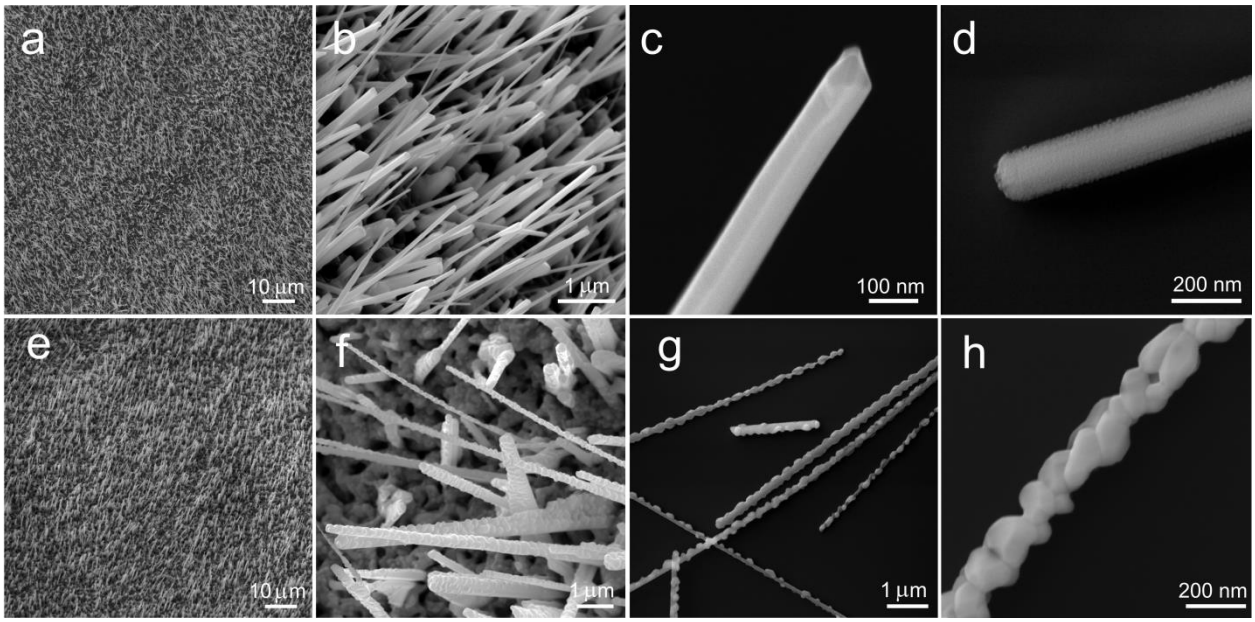

Fig. 3. SEM images of CuO NWs array on copper foil at lower (a) and higher magnification (b), individual CuO NW (c) and WO_3-coated CuO NW (d); core/shell CuO/WO_3 NWs array on copper foil annealed at 650ºC at lower (e) and higher magnification (f). Core/shell CuO/WO_3 NWs on silicon substrate annealed at 650ºC (g, h).

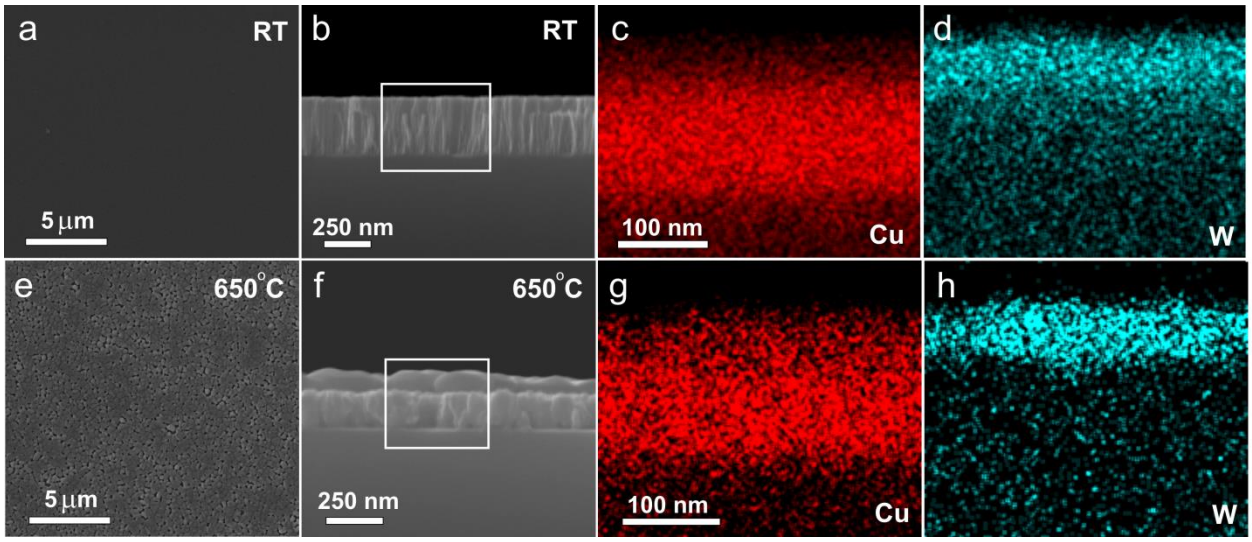

Fig. 4. SEM images of CuO/WO_3 thin film samples deposited on silicon wafer before annealing: top view (a), side view (b) and corresponding EDX maps of Cu and W atom distribution for the selected region (c and d). After annealing at 650º C: top view (e), side view (f) and corresponding EDX maps of Cu and W atom distribution for the selected region (g and h).

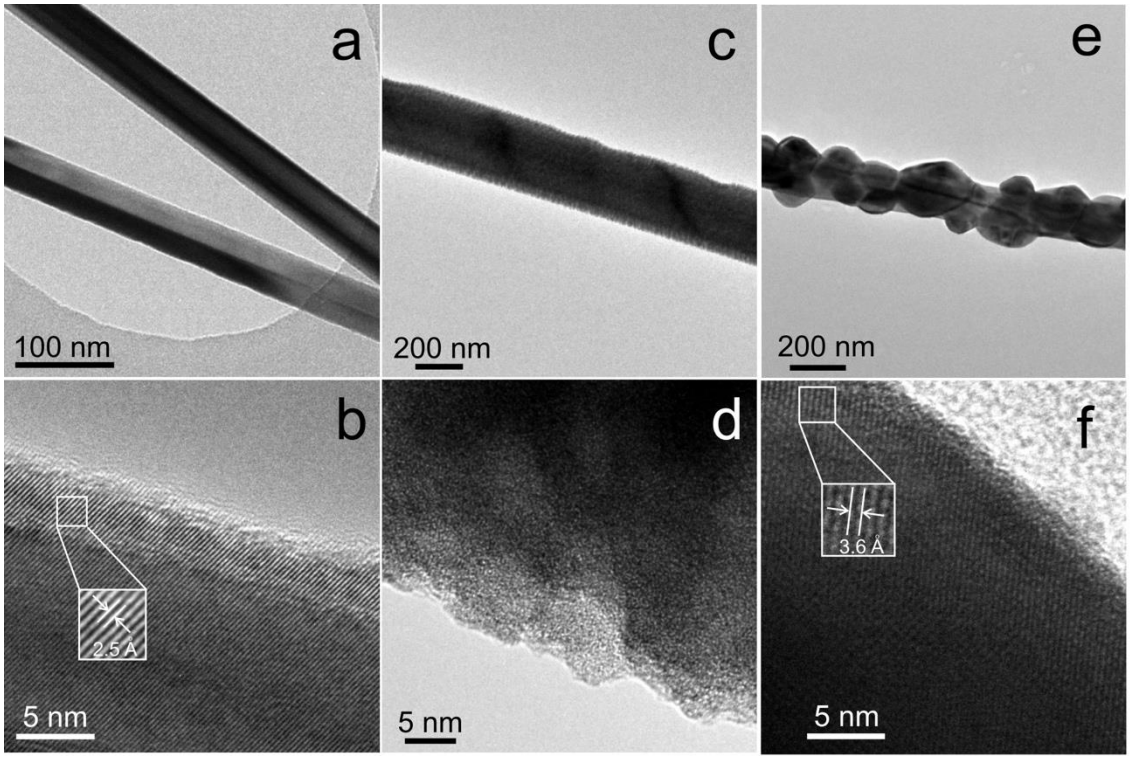

Fig. 5. TEM images at different magnifications of CuO NWs (a, b), core/shell CuO/WO_3 NWs (c, d), core/shell CuO/WO_3 NWs annealed at 650ºC (e, f).

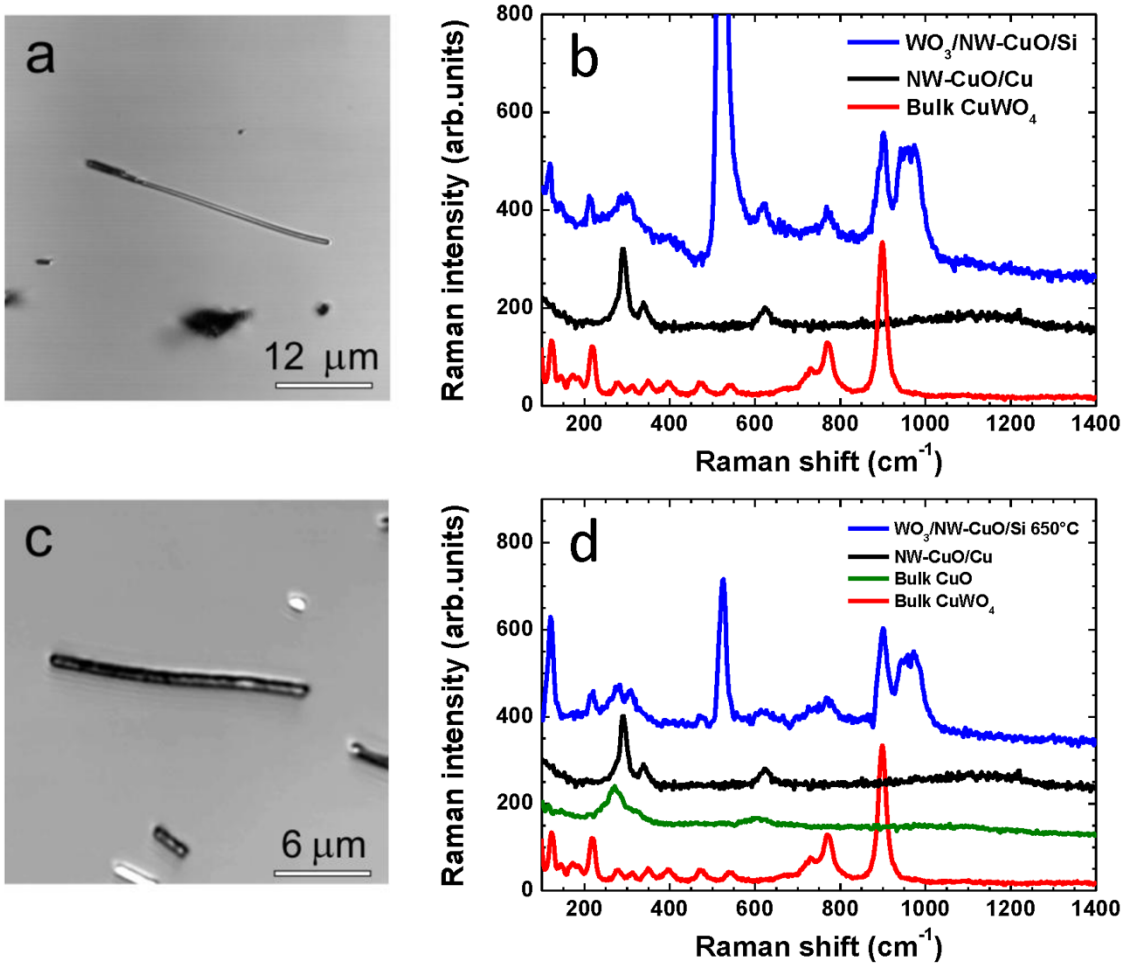

Fig. 6. Confocal microscope images and Raman scattering spectra of core/shell CuO/WO_3 nanowires (NWs) on silicon substrate before (a, b) and after (c, d) annealing at 650ºC. Raman spectra of bulk CuO and $CuWO_4$ powders as well as of CuO NWs on Cu substrate (NW-CuO/Cu) are shown for comparison.

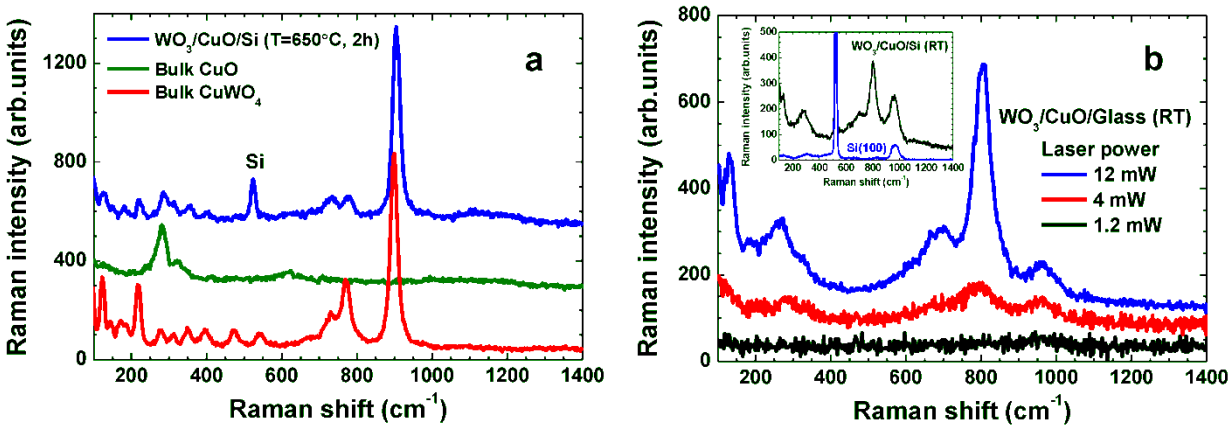

Fig. 7. (a) Raman scattering spectra of CuO/WO_3 thin film on silicon substrate after annealing at 650ºC and of bulk CuO and $CuWO_4$ powders shown for comparison. (b) Raman scattering spectra of as-prepared CuO/WO_3 thin film on glass substrate as a function of laser power (Insert: Raman spectra of as-prepared CuO/WO_3 thin film on silicon substrate and pure silicon substrate).

Institute of Solid State Physics, University of Latvia as the Center of Excellence has received funding from the European Union's Horizon 2020 Framework Programme H2020-WIDESPREAD-01-2016-2017-TeamingPhase2 under grant agreement No. 739508, project CAMART²